

# Preprocessing of hyperspectral imagery with consideration of smile and keystone properties

Naoto Yokoya<sup>\*a</sup>, Norihide Miyamura<sup>b</sup> and Akira Iwasaki<sup>b</sup>

<sup>a</sup>Dept. of Aeronautics and Astronautics, The University of Tokyo, Japan

<sup>b</sup>Research Center for Advanced Science and Technology, The University of Tokyo, Japan

## ABSTRACT

Satellite hyperspectral imaging sensors suffer from “smile” and “keystone” properties, which appear as distortions of spectrum images. The smile property is a center wavelength shift and the keystone property is a band-to-band misregistration. These distortions degrade the spectrum information and reduce classification accuracies. Furthermore, these properties may change after the launch. Therefore, in the preprocessing of satellite hyperspectral images, the onboard correction of the smile and keystone properties is an important issue as well as the radiometric and geometric correction. The main objective of this work is to propose the prototype of the preprocessing of hyperspectral image with consideration of smile and keystone properties. Image registration based on phase correlation is used for detecting the optical properties. Cubic spline interpolation is adopted to modify the spectrum because of its good trade-off between the smoothness and shape preservation. Smile and keystone detection simulation using the EO-1 Hyperion imagery taken at various times in the past nine years proved that the optical properties have been changing due to the onboard secular distortion. Therefore, onboard optical properties should be updated periodically and built into the radiometric and geometric corrections for future satellite hyperspectral sensors. The proposed method may be the prototype of the preprocessing of future satellite hyperspectral sensors.

**Keywords:** hyperspectral imagery, smile, keystone

## 1. INTRODUCTION

Hyperspectral imagers are pushbroom sensors that continuously collect spectrograms that form a three-dimensional (3D) data cube, composed of cross-track ( $x$ ), along-track ( $y$ ), and spectrum ( $\lambda$ ) dimensions, as shown in Figure 1. Hyperspectral imagery contains hundreds to thousands of spectral bands. At each pixel, a continuous spectral profile can be obtained, which enables discrimination among land-cover classes that are spectrally similar [1]. Many spaceborne hyperspectral sensors are developed as the next generation advanced earth observing satellite, such as EnMap (German), PRISMA (Italy), HypSIRI (USA), and HISUI (Japan) [2,3,4,5].

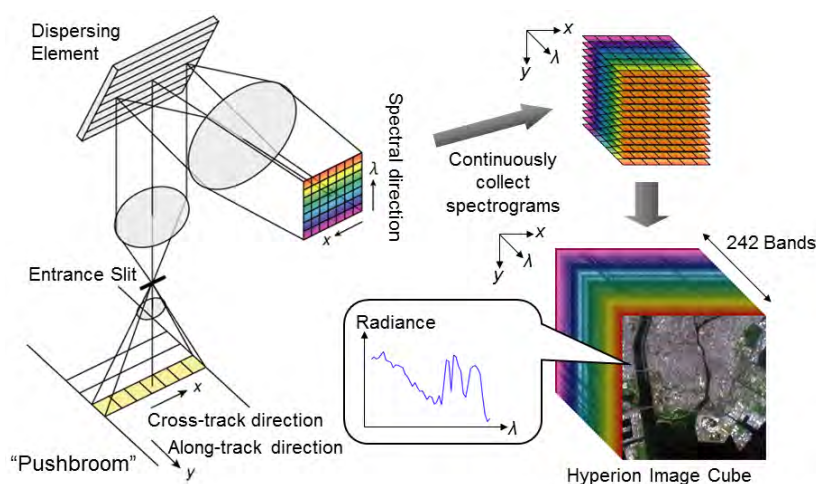


Figure 1. Hyperspectral imaging

\*yokoya@sal.rcast.u-tokyo.ac.jp; phone +81-3-5452-5319

Hyperspectral imageries suffer from sensor optical properties, which distort spectrograms due to optical aberrations and misalignments. These spectrographic distortions cause spectral and spatial misregistrations, commonly called as “smile” and “keystone” properties (Figure 2). Smile property is a shift in wavelength in the spectral domain and keystone property is a band-to-band misregistration. They distort spectral profiles and thus degrade classification results. For example, maximum noise fraction (MNF) transform [6], which produces new components ordered by the signal to noise ratio (SNR), is commonly used for spectral dimensionality reduction of hyperspectral imagery before classification, however, smile effect appears in the first MNF component as a brightness gradient [7]. This artifact is dominant in classification and leads to misclassification [8]. Past studies demanded very high accuracy of optical properties [9,10].

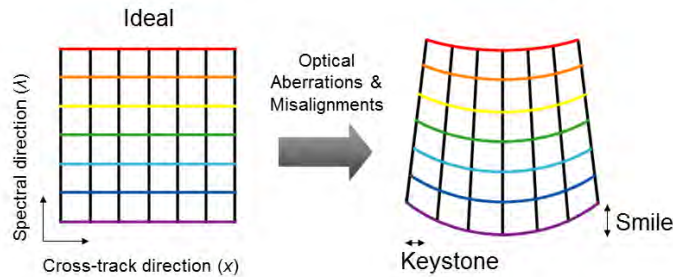


Figure 2. Smile and keystone properties

The Hyperion imaging spectrometer is the first spaceborne hyperspectral sensor that routinely acquires science-grade data mounted on the Earth Observing 1 (EO-1) satellite, which was launched on November 21, 2000. This sensor collects data with a 30 m ground sampling distance over a 7.65-km swath in 198 spectral bands with two spectrometers; the first is the visible near-infrared radiometer (VNIR) over 400-1000 nm, and the other is the shortwave infrared radiometer (SWIR) over 900-2500 nm. The Hyperion data is freely available at the website of U. S. Geological Survey (USGS) (<http://edcscns17.cr.usgs.gov/EarthExplorer/>). Two data formats, L1R and L1Gst, are available. L1R data is radiometrically corrected and L1Gst data is radiometrically corrected and resampled for geometric correction and registration to a geometric map projection with ortho-rectification. Hereafter, we refer to L1Gst as L1G. The Hyperion data contains various noises such as stripe and shot noise and also suffers from smile and keystone properties. Due to these artifacts, classification performance using the Hyperion data was outperformed by those using multispectral data in some cases [11,12]. The prelaunch smile property is attached to the data but the prelaunch keystone property is not. Smile and keystone properties are not corrected in both types of data, L1R and L1G. Moreover, many studies showed that smile property may have changed after the launch. Therefore, building an accurate onboard calibration of optical properties into the L1R and L1G data processing is an important and challenging issue.

The postlaunch smile property was estimated by correlating the sensor-measured spectrum with a spectrum model using moderate resolution atmospheric transmission (MODTRAN) [13,14]. The postlaunch keystone property was detected by a scene-based method based on edge detection using a sharpening filter [15,16]. However, in these past studies, the estimation accuracy and robustness for spatially and temporally different scenes have not yet been evaluated. Recently, we have proposed a methodology for the detection and correction of smile and keystone properties only from observed data [17]. This method is proved to be accurate and robust for various scenes. In this paper, we propose the prototype for the preprocessing of hyperspectral imagery, which produces L1R and L1G data, building in onboard calibration of smile and keystone properties. The Hyperion VNIR data is used as an example. The effect of the onboard calibration of optical properties on L1G data is also demonstrated.

## 2. OVERVIEW FOR L1R AND L1G PROCESSING

Figure 3 shows the flow chart of L1R and L1G data processing which detect and correct the artifacts in hyperspectral imagery. Stripe noise and optical properties are all related to a two-dimensional (2D) detector array and pushbroom imaging system. After the geometric correction, the relationship between the 2D spectroscopic image and the 3D hyperspectral image cube has disappeared. Thus, the removal of these artifacts must be processed before the geometric correction. Since resampling used for data correction degrades spectral signatures, to minimize resampling frequency, smile and keystone correction should be done with radiometric and geometric corrections, respectively.

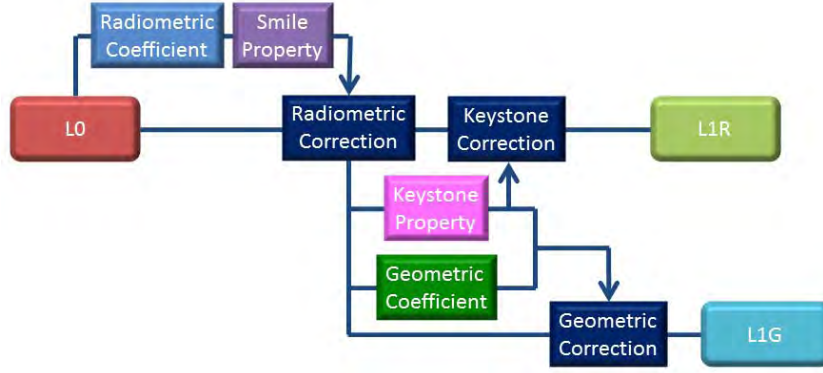


Figure 3. L1R and L1G data processing with consideration of smile and keystone properties.

In the following sections, improvement of radiometric coefficient with stripe noise reduction and accurate onboard calibration of smile and keystone properties are described in details.

### 3. RADIOMETRIC IMPROVEMENT WITH STRIPE NOISE REDUCTION

In the Hyperion imagery, there exist a lot of stripe noises which reduce data quality and interpretability. Almost all of these stripe artifacts are of one pixel width. Several destriping methods have been proposed [18,19], however, these methods are complicated and difficult to replicate accurately. We use the simplest methods for both detection and correction of stripe noise. Stripe noise is a line whose brightness is higher or lower than neighboring lines. Therefore, we detect it using a limit check. Consider a 3D hyperspectral data cube, in which each component located in band  $k$  at cross-track  $i$  and along-track  $j$  position is represented by  $x_{i,j,k}$  ( $1 \leq i \leq W, 1 \leq j \leq H, 1 \leq k \leq B$ ). Here,  $W$  and  $H$  are the width and height and  $B$  is the total number of bands, respectively. In a certain cross-track position  $i$  in band  $k$ , if the total number of pixels, whose brightness is higher or lower than both of cross-track neighboring two pixels, is over a threshold, the line at this cross-track position is detected as a stripe. The total number  $N_{i,j,k}$  is given by

$$N_{i,k} = \sum_j c_{i,j,k},$$

where

$$c_{i,j,k} = \begin{cases} 1 & (x_{i,j,k} < x_{i-1,j,k}, x_{i+1,j,k} \quad \text{or} \quad x_{i,j,k} > x_{i-1,j,k}, x_{i+1,j,k}) \\ 0 & \text{otherwise} \end{cases}.$$

Three sigma limits are used for the threshold. After stripe detection, a moment matching method is applied for stripe noise correction [20]. Moment matching calculates the improved radiometric gain and offset to adjust the average and standard deviation of line radiance to that of the reference line, which is set as the average of neighboring two lines. Each DN is adjusted as follows:

$$DN_{adjusted} = (DN_{initial} - \mu_{i,k}) \frac{\sigma_{reference}}{\sigma_{i,k}} + \mu_{reference}.$$

Here,  $\mu_{i,k}$  and  $\sigma_{i,k}$  denote the average and standard deviation of line radiance located in band  $k$  at cross-track  $i$ , and  $\mu_{reference}$  and  $\sigma_{reference}$  denote those of the reference line. This detection and correction process is repeated until no more stripes are detected. Figure 4 shows the original image, detected stripe, and corrected image for the Hyperion band 57

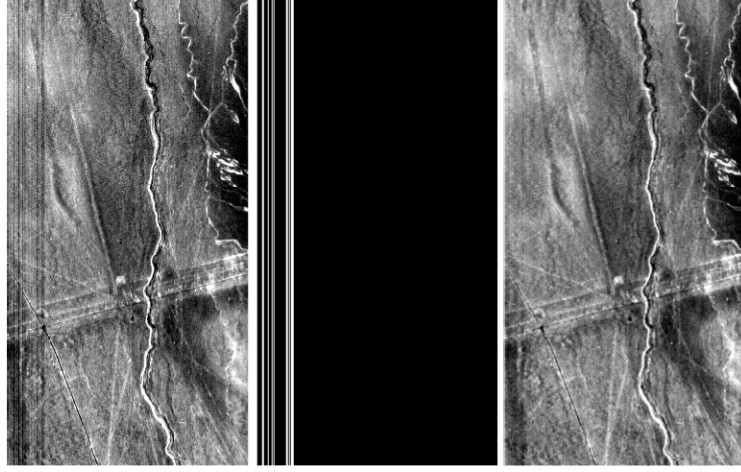


Figure 4. Original image (left), detected stripe (middle), and corrected image (right).

image taken over a desert in Chile. After stripe noise reduction, data quality has improved. Since stripe noise deteriorates smile and keystone detection results, radiometric improvement with stripe noise reduction should be processed before calibration of optical properties.

## 4. ONBOARD CALIBRATION OF SMILE AND KEYSTONE PROPERTIES

### 4.1 Detection and correction methods

Image registration was applied for the accurate detection of onboard optical properties only from observed data [17]. By estimating spectroscopic image distortions in spectral and spatial directions, smile and keystone properties can be detected. In this work, we use image registration based on phase correlation (PC). Consider two  $N_1 \times N_2$  images  $f(n_1, n_2)$  and  $f(n_1 - \delta_1, n_2 - \delta_2)$  that differ only by displacement  $(\delta_1, \delta_2)$ . To reduce the image boundary effect in the frequency domain, a 2D Hanning window is applied to the input image. A low-pass filter is also applied in the frequency domain to eliminate the high-frequency components of image. The simplest low-pass filter is given by  $H(\omega_1, \omega_2) = \{ 1 \leq |\omega_1| \leq U_1, 1 \leq |\omega_2| \leq U_2 \text{ otherwise } 0 \}$ . In this case, the phase correlation  $r(n_1, n_2)$  is simplified by

$$r(n_1, n_2) \cong \alpha \cdot \frac{\sin \frac{V_1}{N_1} \pi(n_1 + \delta_1)}{\pi(n_1 + \delta_1)} \frac{\sin \frac{V_2}{N_2} \pi(n_2 + \delta_2)}{\pi(n_2 + \delta_2)},$$

where  $\alpha \leq 1$ ,  $V_1 = 2U_1 + 1$  and  $V_2 = 2U_2 + 1$ . The value of displacement  $(\delta_1, \delta_2)$  and the value  $\alpha$  can be obtained independently, assuming that one misregistration is fixed. Thus, for mathematical simplicity, an 1D version of the correlation function is considered in the following description. The 1D correlation function is given by

$$r(n) \cong \beta \cdot \frac{\sin \frac{V}{N} \pi(n + \delta)}{\pi(n + \delta)}.$$

The displacement can be obtained in the subpixel level by estimating the peak location of the correlation function. Using sinc function fitting, the subpixel value of the displacement is directly obtained by

$$\delta = \frac{r(n_0 - 1) - r(n_0 + 1)}{r(n_0 - 1) - 2 \cos\left(\pi \frac{V}{N}\right) r(n_0) + r(n_0 + 1)},$$

where  $n_0$  is the integer with the maximum value of correlation function [21].

For the smile and keystone correction, we use cubic spline interpolation because of its good trade-off between smoothness and shape preservation [22]. Sinc function interpolation coded in MATLAB with a not-a-knot end condition is applied to hyperspectral data cube in the spectral and cross-track directions to modify smile and keystone properties, respectively.

## 4.2 Smile property

Smile effect was estimated by applying image registration based on phase correlation to a spectroscopic image in the cross-track direction. The size of correlation window  $(L_x, L_\lambda)$  is set as (1,11), where  $L_x$  and  $L_\lambda$  are the lengths in cross-track and spectral direction, respectively. Since bands 1-7 and 58-70 of the Hyperion imagery have no data and correlation window is wide in the spectral direction, we estimate smile effect in bands 13-52. Nine scenes taken over Sahara desert in 2002 to 2010 are used as examples because spectral signature should be homogeneous in cross-track direction for smile detection. We estimate smile effect for each along-track position and return the average result as the final smile effect. Figure 5 shows the estimated smile effect of bands 13-52 for nine desert scenes. The bottom number denotes the data acquisition date; the first number is the year and the second is the number of days elapsed from January 1<sup>st</sup>. Smile property can be detected when a spectral signature in the correlation window contains a clear atmospheric absorption line [17]. Therefore, smile property in band 41, which is an oxygen absorption line, can be detected. Smile property can be approximated as a quadratic function. Figure 6 shows secular change appearing in cross-track position in band 41 smile axis. Smile property has been changing after the launch with a certain tendency. It indicates that periodical update of smile property is necessary for satellite hyperspectral sensor. According to MNF transform analysis, the smile effect in band 41 clearly appears in the difference image between bands 40 and 42. Figure 7 shows comparison of this difference image between before and after smile effect correction. Smile brightness gradient in the spectral direction disappears after smile correction. Figure 8 shows the difference image between bands 40 and 42 in L1G data format taken over San Francisco. Brightness gradient also disappears in L1G, which shows that smile correction before geometric correction improved the quality of L1G data. Thus, the L1G data product can be distributed to users after smile correction. There is no or little smile effect in bands 13-34. It may be because radiometric correction in bands 13-34 was not carried out accurately. It suggests that radiometric coefficient and smile property should be iteratively estimated for a number of times.

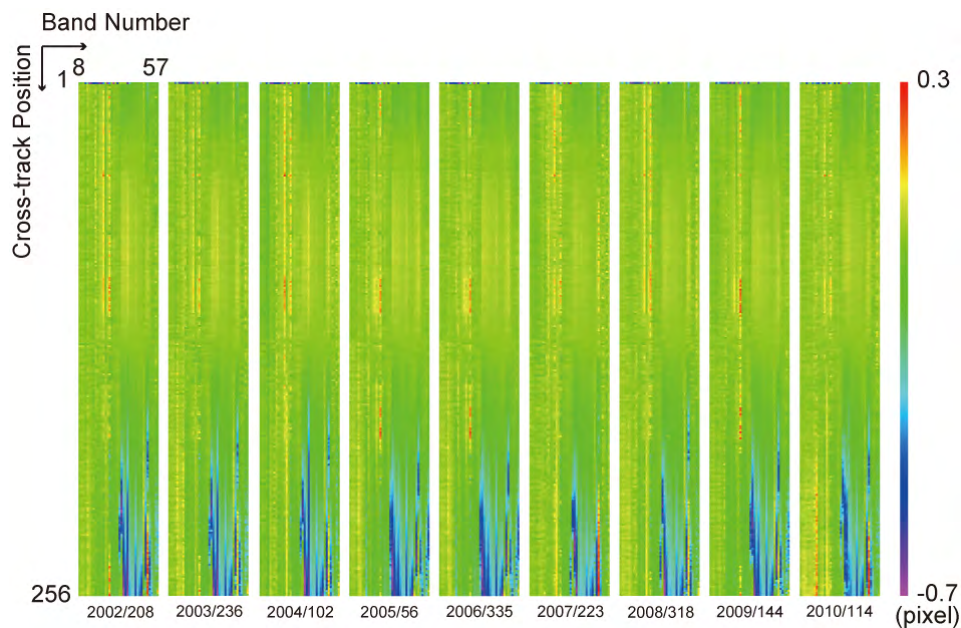


Figure 5. Smile effect estimated for various nine imagery taken over Sahara desert in 2002-2010.

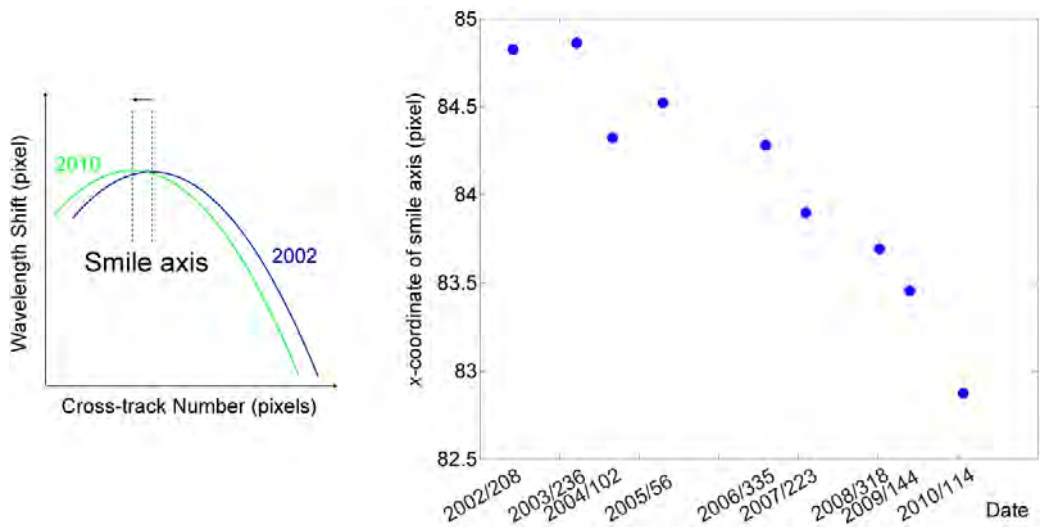


Figure 6. Secular change of band 41 smile property appearing in cross-track position of smile axis.

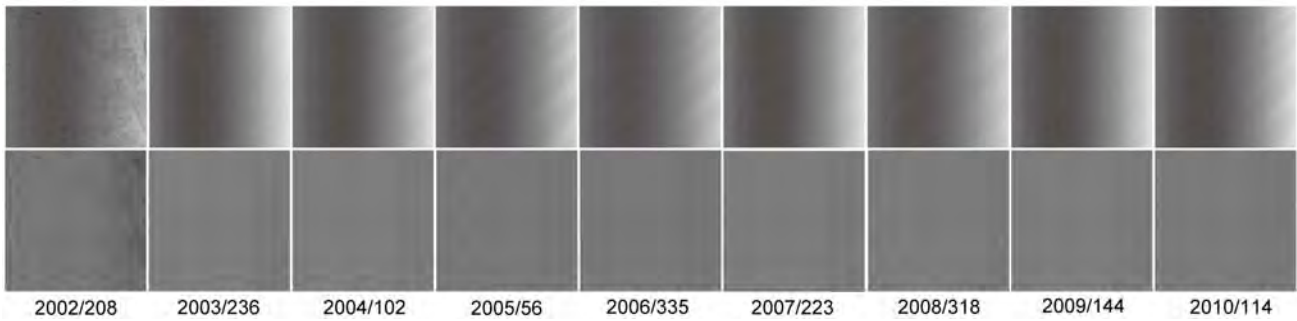


Figure 7. Radiance difference images between bands 40 and 42 before (upper images) and after (lower images) smile correction for various nine imagery taken over Sahara desert in 2002-2010.



Figure 8. Radiance difference between bands 40 and 42 before (middle) and after (right) smile correction in L1G data.

### 4.3 Keystone property

Keystone property was detected at each cross-track position by applying image registration to a small hyperspectral cube in the spectral direction and estimating band-to-band misregistrations. The size of the correlation window  $(L_x, L_y)$  is set to  $(31,31)$ , where  $L_x$  and  $L_y$  are the lengths in cross-track and along-track direction, respectively. Phase correlation method assumes that input and reference images are almost the same. Desert scenes with clear texture were used as examples because there were no contrast conversions such as vegetation, and texture of each band was almost the same. The average result of detected keystone properties at all along-track positions was defined as the final detected keystone property. Figure 9 shows the comparison of images before and after keystone property detection for nine desert scenes also used for smile property, especially using imagery taken over ripple marks. The Maximum band-to-band misregistration that was about 10-20% of spatial resolution before keystone correction reduced to within 5%. The Hyperion keystone property can be approximated as a linear function. Figure 10 shows the secular change of keystone slope. There is also a certain tendency consistent with that of smile property. It strongly suggests that optical properties of the Hyperion may have varied across the days after the launch. Therefore, an onboard periodical update of optical properties built into L1R and L1G data processing is necessary for future satellite hyperspectral sensors.

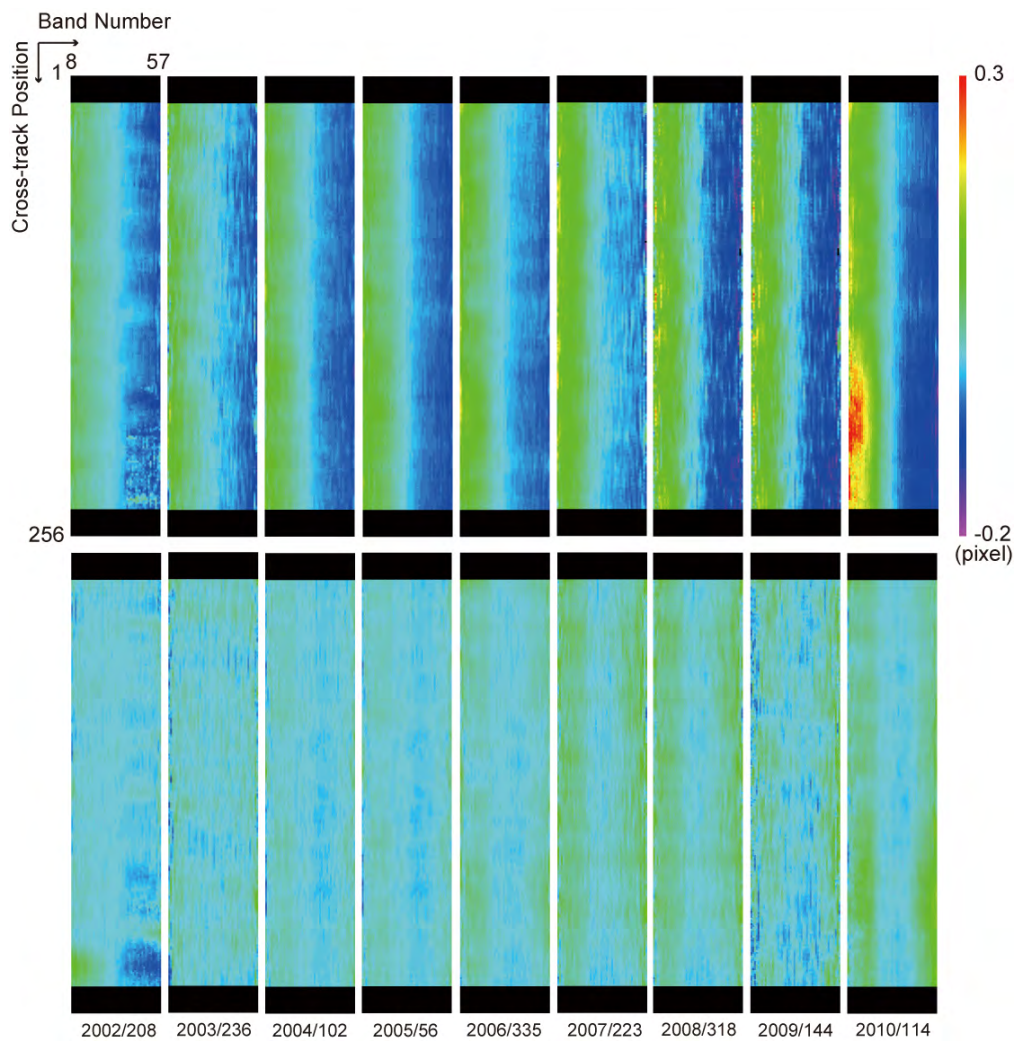


Figure 9. Keystone properties before (upper images) and after (lower images) keystone correction estimated for various nine imagery taken over Sahara desert in 2002-2010.

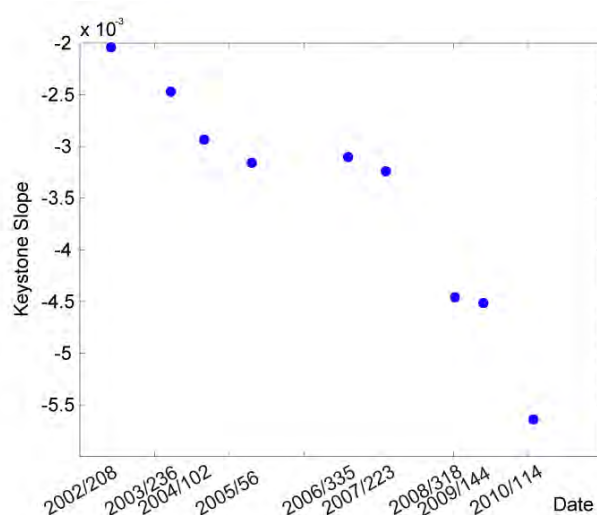


Figure 10. Secular change of keystone slope.

## 5. CONCLUSION

In this work, we proposed the L1R and L1G data processing of hyperspectral imagery with consideration of smile and keystone properties. Image registration based on phase correlation is used for detection of smile and keystone properties and cubic spline interpolation is applied for correction of spectral signatures. Smile correction should be built into radiometric correction. Furthermore, keystone correction should be processed together with geometric correction. Smile and keystone detection simulation using the EO-1 Hyperion imagery taken at various times in the past nine years demonstrated that the optical properties have been changing due to the onboard secular distortion. Therefore, onboard optical properties should be updated periodically and built into L1R and L1G data processing for future satellite hyperspectral sensors.

## REFERENCES

- [1] Kruse, F. A., Boardman, J. W., and Huntington, J. F., "Comparison of airborne hyperspectral data and EO-1 Hyperion for mineral mapping," *IEEE Trans. Geosci. Remote Sens.* 41(6), 1388-1400 (2003).
- [2] Sang, B., Schubert, J., Kaiser, S., Mogulsky, V., Neumann, C., Förster, K., Hofer, S., Stuffer, T., Kaufmann, H., Müller, A., Eversberg, T., Chlebek C., "The EnMAP hyperspectral imaging spectrometer: instrument concept, calibration and technologies," *Proc. SPIE 7086*, 708605 (2008).
- [3] Galeazzi, C., Sacchetti, A., Cisbani, A., Babini, G., "The PRISMA program," *Proc. IEEE International Geoscience and Remote Sensing Symposium 4*, 105-108 (2008).
- [4] Chien, S., Silverman, D., Davies, A. G., Mandl, D., "Onboard science processing concepts for the HypSPIRI mission," *IEEE Intelligent Systems* 24(6), 12-19 (2009).
- [5] Ohgi, N. and Iwasaki A., "Japanese hyper-multi spectral mission," *Proc. IEEE International Geoscience and Remote Sensing Symposium* (2010).
- [6] Green, A. A., Berman, M., Switzer, P., and Craig, M. D., "A transformation for ordering multispectral data in terms of image quality with implications for noise removal," *IEEE Trans. Geosci. Remote Sens.* 26(1), 65-74 (1988).
- [7] Goodenough, D. G., Dyk, A., Niemann, K. O., Pearlman, J. S., Chen, H., Han, T., Murdoch, M., and West, C., "Processing Hyperion and ALI for forest classification," *IEEE Trans. Geosci. Remote Sens.* 41(6), 1321-1331 (2003).

- [8] Dadon, A., Ben-Dor, E., and Karnieli, A., "Use of derivative calculations and minimum noise fraction transform for detecting and correcting the spectral curvature effect (smile) in Hyperion images," *IEEE Trans. Geosci. Remote Sens.* 48(6), 2603-2612 (2010).
- [9] Green, R. O., "Spectral calibration requirement for Earth-looking imaging spectrometers in the solar-reflected spectrum," *Appl. Opt.* 37(4), 683-690 (1998).
- [10] Mouroulis, P., Green, R. O., and Chrien, T. G., "Design of pushbroom imaging spectrometers for optimum recovery of spectroscopic and spatial information," *Appl. Opt.* 39(13), 2210-2220 (2000).
- [11] Waldhoff, G., Bubenzer, O., Bolten, A., Koppe, W., and Bareth, G., "Spectral analysis of ASTER, Hyperion, and QuickBird data for geomorphological and geological research in Egypt (Dakhla Oasis, Western Desert)," in *Proc. XXI ISPRS Congress, Commission VIII, XXXVIII-B8*, 1201-1206 (2008).
- [12] Gordley, L., Marshall, B., McHugh, M., Fritts, D., and Fish, C., "Spectral analysis of ASTER and Hyperion data for geological classification of Volcano Teide," *Proc. IEEE International Geoscience and Remote Sensing Symposium* (2010).
- [13] Pearlman, J. S., Barry, P. S., Segal, C. C., Shepanski, J., Beiso, D., and Carman, S. L., "Hyperion, a space-based imaging spectrometer," *IEEE Trans. Geosci. Remote Sens.* 41(6), 1160-1173 (2003).
- [14] Neville, R. A., Sun, L., and Staenz, K., "Detection of spectral line curvature in imaging spectrometer data," *Proc. SPIE* 5093, 144-154 (2003).
- [15] Neville, R. A., Sun, L., and Staenz, K., "Detection of keystone in imaging spectrometer data," *Proc. SPIE* 5425, 208-217 (2004).
- [16] Dell'Endice, F., Nieke, J., Schlapfer, D., and Itten, K. I., "Scene-based method for spatial misregistration detection in hyperspectral imagery," *Appl. Opt.* 46(15), 2803-2816 (2007).
- [17] Yokoya, N., Miyamura, N., and Iwasaki, A., "Detection and correction of spectral and spatial misregistrations for hyperspectral data using phase correlation method," *Appl. Opt.* 49(24), 4568-4575 (2010).
- [18] Tsai, F., and Chen, W. W., "Striping noise detection and correction of remote sensing images," *IEEE Trans. Geosci. Remote Sens.* 46(12), 4122-4131 (2008).
- [19] Sun, L., Neville, R. A., Staenz, K., and White, H. P., "Automatic destriping of Hyperion imagery based on spectral moment matching," *Can. J. Remote Sens.* 34(1), S68-S81 (2008).
- [20] Gadallah, F. L., Csillag, F. and Smith, E. J. M., "Destriping multisensor imagery with moment matching," *Int. J. Remote Sens.*, 21(12), 2505-2511 (2000).
- [21] Nagashima, S., Aoki, T., Higuchi, T., and Kobayashi, K., "A subpixel image matching technique using phase-only correlation," *Proc. IEEE International Symposium on Intelligent Signal Processing and Communication Systems*, 701-704 (2006).
- [22] Feng, Y. and Xiang, Y., "Mitigation of spectral mis-registration effects in imaging spectrometers via cubic spline interpolation," *Opt. Express* 16(20), 210-221 (2002).